Proc. of SPIE Vol. 0450, Structural Mechanics of Optical Systems I, ed. L.M. Cohen (Jan 1983) Copyright SPIE

Flat circular optical elements on a 9-point Hindle mount in a 1-g force field

Pravin K. Mehta

Electro-Optical Division, Perkin-Elmer Corporation, Mail Station 955
100 Wooster Heights Road, Danbury, Connecticut 06810

Abstract

The problem of supporting an optical element in a 1-g force field on a multi-level kinematic mount arises, when a single level 3-point kinematic mount is inadequate for keeping the stress and/or surface deflection within specified design limits. In this paper, a solution of the biharmonic differential equation for the bending of a flat thin circular plate is first derived for m-point ($m \geq 2$) supports, equi-spaced on a concentric circle, and then applied to the problem of a two-level kinematic mount, which is also known as a 9-point Hindle mount. From this, normalized design curves are developed for determining nominal locations of the nine support points, associated RMS deflections and support location sensitivity. These design curves provide the practicing engineer with a useful, efficient and accurate means for developing a preliminary Hindle mount design without resorting to FEM analysis. Several cases of the 9-point Hindle mount solution were compared with independent NASTRAN based finite element solutions. Excellent correlation between the two was obtained in all cases. The methodology used in this paper is not limited to flat optical elements. The solution of the problem of curved optical elements on a 9-point Hindle mount in a 1-g force field can be similarly obtained by the same approach with E. Reissner's thin shallow spherical shell equations.

Introduction

A 9-point Hindle mount, shown schematically in Figure 1 with symmetric delta-plates, is a two-level kinematic mount. The first level consists of nine mounting points on the back surface of the optical element. These points are attached to the vertices of three triangular mounting plates, sometimes known as delta-plates, by means of axially (z axis) stiff but otherwise compliant support posts. The centroids of three delta-plate constitute the second level of supports. Each of them is mounted on a universal joint and is fixed in axial translation. Such a mounting arrangement permits the optical elements to deflect at the nine support points of the first level, which may accordingly be called the "floating" supports in contrast to the three "fixed" supports of the second level. Furthermore, the reactions at all the support points can be determined kinematically from the equations of static equilibrium. Each of the floating support nominally provides a reaction equal to W/9, where W is the weight of the optical element, provided that $s_0 = (2s_2 \cos \phi_2 + s_3)/3$ in Figure 1. The reaction at each fixed support is W/3.

Of interest to the design engineer are not only the deflection function $w = w(r,\theta)$ of the optical element and the associated RMS figure error for the nominal Hindle mount support configuration of Figure 1, but also the effect of off-nominal deviations of the

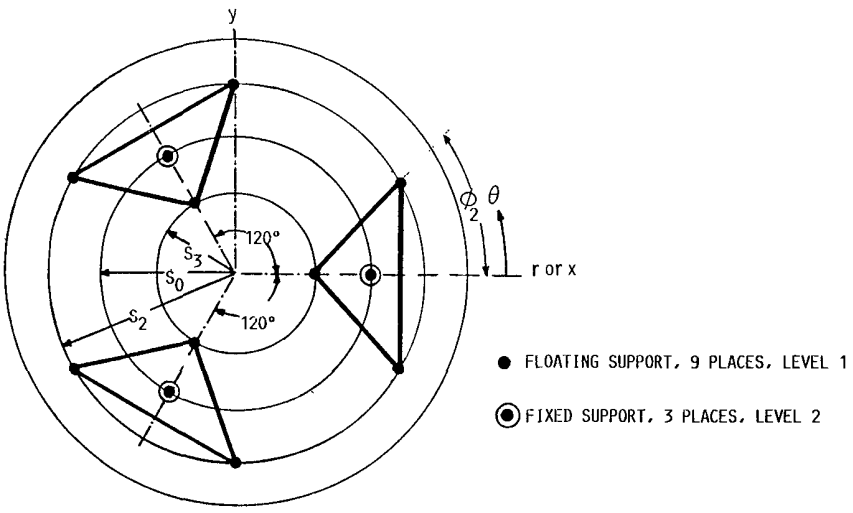

Figure 1. A schematic representation of a 9-point Hindle mount with symmetric delta-plates

support locations for establishing allowable tolerances on them. Accordingly, for the location sensitivity analysis, the three floating supports and one fixed support constituting a delta-plate are perturbed from their nominal positions as shown in Figure 2. For simplicity, the perturbations of corresponding support points in all three delta-plates are assumed to be identical. Specifically, for a given value of i, the corresponding

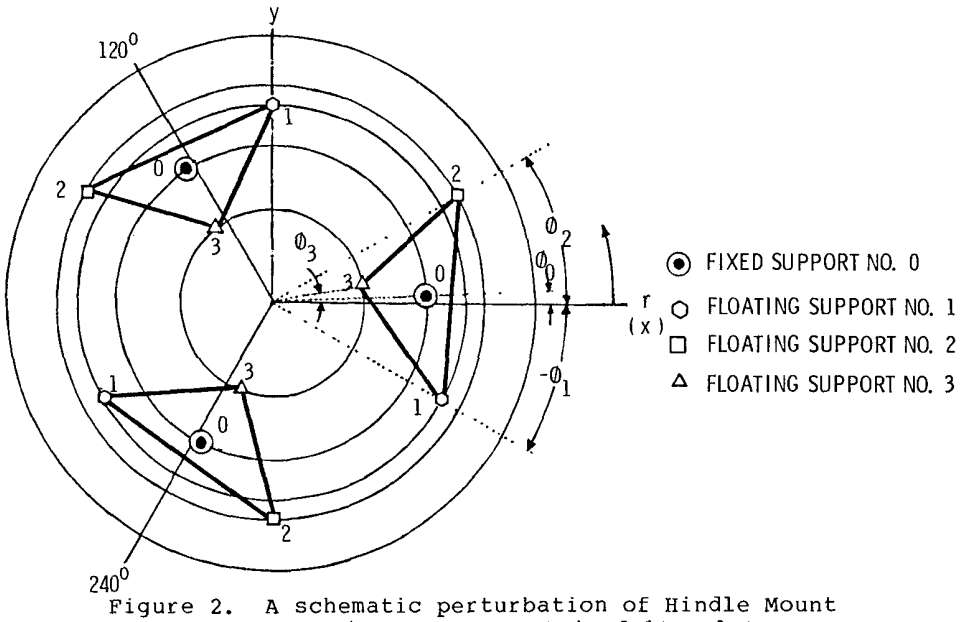

Figure 2. A schematic perturbation of Hindle Mount support locations; nonsymmetric delta-plates

support point in each delta-plate lies on the same pitch circle and is azimuthally spaced 120° from the other two (one on each side). Thus the three fixed supports, denoted by i = 0, lie on a pitch circle of radius s_o and are located at $\theta = \phi_o$, $\phi_o + 120^o$ and $\phi_o + 240^o$, respectively. Similarly, the three floating supports, denoted by i = 1, lie on a pitch circle of radius s_1 and are located at $\theta = \phi_1$, $\phi_1 + 120^o$ and $\phi_1 + 240^o$, respectively, and so on.

Analytical approach

Since the nominal case of Figure 1 is only a subset of the general case of Figure 2, we need to develop the analysis only for the Hindle mount with nonsymmetric delta-plates. Then by making $s_1 = s_2$, $\phi_1 = -\phi_2$ and $\phi_o = \phi_3 = 0$, the entire analysis will be applicable to the nominal case with symmetric delta-plates.

The nonsymmetric case can be viewed as a superposition of three subcases, each consisting of the same optical element on different sets of 3-point supports and subjected to a different unknown applied load. A 3-point support set consists of floating point i in each delta-plate and i = 1, 2, or 3. For the determination of applied load in each subcase, let us consider the equilibrium of any delta-plate. Denoting the floating support reactions by P_i, we have

$$\sum F_z = \sum_{i=1}^{3} P_i = W/3 \tag{1}$$

$$\sum M_x = \sum_{i=1}^{3} P_i s_i \sin \phi_i - (W/3) s_o \sin \phi_o = 0 \tag{2}$$

$$\sum M_y = \sum_{i=1}^{3} P_i s_i \cos \phi_i - (W/3) s_o \cos \phi_o = 0 \tag{3}$$

Solving these three equations, we have $P_i = \mu_i W/3$ (for i = 1, 2 and 3), where

$$\mu_1 = \frac{s_2 s_3 \sin(\phi_2-\phi_3) - s_o\left[s_2 \sin(\phi_2-\phi_o) - s_3 \sin(\phi_3-\phi_o)\right]}{s_1 s_2 \sin(\phi_1-\phi_2) + s_2 s_3 \sin(\phi_2-\phi_3) + s_3 s_1 \sin(\phi_3-\phi_1)} \tag{4}$$

$$\mu_2 = \frac{s_3 s_1 \sin(\phi_3-\phi_1) - s_o\left[s_3 \sin(\phi_3-\phi_o) - s_1 \sin(\phi_1+\phi_o)\right]}{s_1 s_2 \sin(\phi_1-\phi_2) + s_2 s_3 \sin(\phi_2-\phi_3) + s_3 s_1 \sin(\phi_3-\phi_1)} \tag{5}$$

$$\mu_3 = \frac{s_1 s_2 \sin(\phi_1-\phi_2) - s_o\left[s_1 \sin(\phi_1+\phi_o) - s_2 \sin(\phi_2-\phi_o)\right]}{s_1 s_2 \sin(\phi_1-\phi_2) + s_2 s_3 \sin(\phi_2-\phi_3) + s_3 s_1 \sin(\phi_3-\phi_1)} \tag{6}$$

It may be noted that, in these expressions for μ_i, ϕ_1 is negative, while ϕ_o, ϕ_2 and ϕ_3 are positive as indicated in Figure 2. In general, angles measured counter-clockwise from the reference line $\theta = 0$ are positive, while those measured clockwise are negative. The total applied load for each subcase is $3P_i = \mu_i W$ and is uniformly distributed.

The problem of self-weight induced distortion of an optical element on a 9-point Hindle mount is then equivalent to the superposition of three subcases in each of which the optical element is uniformly loaded by a total applied load $\mu_i W$ and is supported at three points. In this paper, a solution of the biharmonic differential equation[1] of a flat thin circular plate, with and without a central hole and supported on m-points ($m \geq 2$) symmetrically equi-spaced on a concentric circle, is applied to flat circular optical elements on a 9-point Hindle mount. The similar problem of curved circular optical elements will be treated with E. Reissner's shallow spherical shell equations[2] in a future publication.

Solution for multi-point support

The biharmonic differential equation for the bending of a thin flat circular plate is given by

$$\nabla^2 \nabla^2 w = pa^4/D, \tag{7}$$

where ∇^2 = Laplacian operator = $\partial^2/\partial\rho^2 + 1/\rho\partial\rho + \partial^2/\rho^2\partial\theta^2$, w = plate deflection, D = flexural rigidity of the plate, a = plate outer radius, p = applied load intensity, and $\rho = r/a$ = normalized radial coordinate. For a uniform applied pressure $p = p_o$, the general solution of Eq. (7) is[1]

$$w = \sum_{n=o}^{\infty} w_{h_n} \cos n\theta + \sum_{n=1}^{\infty} \hat{w}_{h_n} \sin n\theta + p_o \rho^4 a^4/64D, \tag{8}$$

where

$$w_{h_o} = A_o + B_o\rho^2 + C_o \ln \rho + D_o\rho^2 \ln \rho \tag{9}$$

$$w_{h_1} = A_1\rho + B_1\rho^3 + C_1\rho^{-1} + D_1\rho \ln \rho \tag{10}$$

$$w_{h_n} = A_n\rho^n + B_n\rho^{n+2} + C_n\rho^{-n} + D_n\rho^{-(n-2)}, \quad n \geq 2 \tag{11}$$

$$\hat{w}_{h_1} = \hat{A}_1\rho + \hat{B}_1\rho^3 + \hat{C}_1\rho^{-1} + \hat{D}_1\rho \ln \rho \tag{12}$$

$$\hat{w}_{h_n} = \hat{A}_n\rho^n + \hat{B}_n\rho^{n+2} + \hat{C}_n\rho^{-n} + \hat{D}_n\rho^{-(n-2)}, \quad n \geq 2 \tag{13}$$

and A_o, B_o,...., $\hat{C}_n$, $\hat{D}_n$ are integration constants.

For a uniformly loaded circular plate on a multi-point support schematically shown in Figure 3, it can be shown that we need to retain only cos nθ terms from the general solution represented by Eq. (8). Further, if the number of supports, which are assumed to be equi-spaced on a concentric support circle of radius c, is m (m ⩾ 2), then only those cos nθ terms in which n = m, 2m, 3m, ... need to be retained in the general solution.

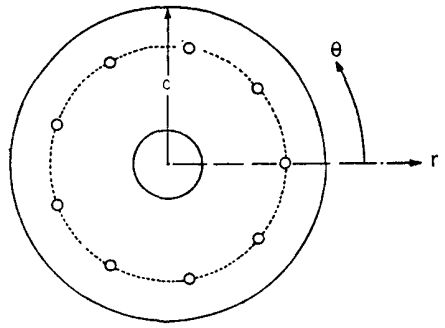

Figure 3. A schematic representation of m-point (multi-point) mount, m ≥ 2

Let P_j = reaction at support j, where j = 1, 2, ..., m. Using for P_j an expression in the form of an infinite series

$$\frac{P_j}{\pi c}\left[\frac{1}{2} + \sum_{n=1}^{\infty} \cos n \left(\theta - \frac{(j-1)2\pi}{m}\right)\right] \tag{14}$$

and since by symmetry

$$P_1 = P_2 = \ldots\ldots = P_m = P, \tag{15}$$

we have for the sum of the reactions

$$\sum_{j=1}^{m} P_j = \frac{P}{\pi c}\left[\frac{m}{2} + \sum_{n=1}^{\infty}\sum_{j=1}^{m} \cos n \left(\theta - \frac{2\pi(j-1)}{m}\right)\right]$$

$$= \frac{P}{\pi c}\left[\frac{m}{2} + \sum_{n=1}^{\infty}\left(\sum_{j=1}^{m} \cos\frac{2\pi n(j-1)}{m}\right)\cos n\theta + \sum_{n=1}^{\infty}\left(\sum_{j=1}^{m} \sin\frac{2\pi n(j-1)}{m}\right)\sin n\theta\right]$$

If n = km, where k = 1, 2, 3, ...,

$$\sum_{j=1}^{m} \cos\frac{2\pi n(j-1)}{m} = \sum_{j=1}^{m} \cos 2\pi k(j-1) = m,$$

$$\sum_{j=1}^{m} \sin\frac{2\pi n(j-1)}{m} = \sum_{j=1}^{m} \sin 2\pi k(j-1) = 0$$

If n ≠ km, where k = 1, 2, 3, ...,

$$\sum_{j=1}^{m} \cos\frac{2\pi n(j-1)}{m} = \sum_{j=1}^{m} \sin\frac{2\pi n(j-1)}{m} = 0,$$

Therefore,

$$\sum_{j=1}^{m} p_j = \frac{P}{\pi c}\left[\frac{m}{2} + \sum_{n=m,2m,3m,\ldots..}^{\infty} m\cos n\theta\right] \tag{16}$$

In view of the uniformly applied load and the form of the sum of support reactions given by Eq. (16), only the cos nθ terms in which n = m, 2m, 3m, ..., should be retained in the general solution given by Eq. (8). Accordingly, the general solution for the multi-point support problem under consideration is given by

$$w = \sum_{k=o}^{\infty} w_{h_n} \cos n\theta + p_o\rho^4 a^4/64D, \qquad n = km, \tag{17}$$

where w_{h_n} is given by Eq. (9) when n = 0, and by Eq. (11) when n ≥ 2.

Deflection functions and stress resultants

Let b = radius of the central hole in the plate, ρ_b = b/a and ρ_c = c/a, where c = support circle radius shown in Figure 3. Also let the stress resultants per unit length be denoted as follows: M_r = radial bending moment, M_t = tangential bending moment, M_{rt} = torsional bending moment, Q_r = radial transverse shear force, Q_t = tangential transverse shear force and V = support reaction. Then the deflection, slope and curvature functions and the stress resultants for the inner and outer regions of the circular plate are as follows:

Inner region, $\rho_b \leq \rho \leq \rho_c$: First for n = 0, we have

$$w_o = A_o + B_o\rho^2 + C_o \ln \rho + D_o\rho^2 \ln \rho + p_o\rho^4a^4/64D \tag{18}$$

$$\partial w_o/\partial r = \left[2B_o\rho + C_o/\rho + D_o\rho(1 + 2 \ln \rho)\right]/a + p_o\rho^3a^3/16D \tag{19}$$

$$\partial^2 w_o/\partial r^2 = \left[2B_o - C_o/\rho^2 + D_o(3 + 2 \ln \rho)\right]/a^2 + 3p_o\rho^2a^2/16D \tag{20}$$

$$M_{r_o} = -\left[2B_o(1 + \nu) - C_o(1 - \nu)/\rho^2 + D_o\{(3 + \nu) + 2(1 + \nu) \ln \rho\}\right] D/a^2 - p_o(3+\nu)\rho^2a^2/16 \tag{21}$$

$$M_{t_o} = -\left[2B_o(1 + \nu) + C_o(1 - \nu)/\rho^2 + D_o\{(1+3\nu) + 2(1+\nu) \ln \rho\}\right] D/a^2 - p_o(1+3\nu)\rho^2a^2/16 \tag{22}$$

$$M_{rt_o} = Q_{t_o} = 0 \tag{23}$$

$$Q_{r_o} = -\left[4D_o/\rho\right] D/a^3 - p_o\rho\, a/2 \tag{24}$$

$$V_o = Q_{r_o} \tag{25}$$

Next for n = km $\geq$ 2 (k = 1, 2, 3, ...), we have

$$w_n = \left[A_n\rho^n + B_n\rho^{n+2} + C_n\rho^{-n} + D_n\rho^{-(n-2)}\right] \cos n\theta \tag{26}$$

$$\partial w_n/\partial r = \left[\{A_n n\rho^{n-1} + B_n(n+2)\rho^{n+1} - C_n n\rho^{-(n+1)} - D_n(n-2)\rho^{-(n-1)}\}/a\right] \cos n\theta \tag{27}$$

$$\partial^2 w_n/\partial r^2 = \left[\{A_n n(n-1)\rho^{n-2} + B_n(n+1)(n+2)\rho^n + C_n\, n(n+1)\rho^{-(n+2)} + D_n(n-1)(n-2)\rho^{-n}\}/a^2\right] \cos n\theta \tag{28}$$

$$M_{r_n} = -\left[A_n n(n-1)(1-\nu)\rho^{n-2} + B_n(n+1)\{(n+2) - \nu(n-2)\}\rho^n + C_n n(n+1)(1-\nu)\rho^{-(n+2)} + D_n(n-1)\{(n-2) - \nu(n+2)\}\rho^{-n}\right](D/a^2) \cos n\theta \tag{29}$$

$$M_{t_n} = \left[A_n n(n-1)(1-\nu)\rho^{n-2} + B_n(n+1)\{(n-2) - \nu(n+2)\}\rho^n + C_n n(n+1)(1-\nu)\rho^{-(n+2)} + D_n(n-1)\{(n+2) - \nu(n-2)\}\rho^{-n}\right](D/a^2) \cos n\theta \tag{30}$$

$$M_{rt_n} = -\Big[A_n n(n-1)\rho^{n-2} + B_n n(n+1)\rho^{n} - C_n n(n+1)\rho^{-(n+2)} - D_n n(n-1)\rho^{-n}\Big]\Big[D(1-\nu)/a^2\Big] \sin n\theta \tag{31}$$

$$Q_{r_n} = -\Big[4B_n n(n+1)\rho^{n-1} + 4D_n n(n-1)\rho^{-(n+1)}\Big](D/a^3) \cos n\theta \tag{32}$$

$$Q_{t_n} = -\Big[4B_n n(n+1)\rho^{n-1} - 4D_n n(n-1)\rho^{-(n+1)}\Big](D/a^3) \sin n\theta \tag{33}$$

$$V_n = n\Big[A_n n(n-1)(1-\nu)\rho^{n-3} - B_n(n+1)\{4-n(1-\nu)\}\rho^{n-1} - C_n n(n+1)(1-\nu)\rho^{-(n+3)} - D_n(n-1)\{4+n(1-\nu)\}\rho^{-(n+1)}\Big](D/a^3) \cos n\theta \tag{34}$$

Outer region, $\rho_c \leq \rho \leq 1$: For the outer region, the expressions for deflection, slope and curvature functions and the stress resultants are obtained from those of the inner region, Eqs. (18) through (34), by replacing the integration constants A_o, B_o, ..., C_n, D_n with constants $\bar{A}_o$, $\bar{B}_o$, ..., $\bar{C}_n$, $\bar{D}_n$, respectively, and denoting the deflection by $\bar{w}$ and stress resultants by $\bar{M}_r$, $\bar{M}_t$, $\bar{Q}_r$, $\bar{Q}_t$ and $\bar{V}$, respectively.

Continuity Conditions

The integration constants for the two regions are related by the conditions of continuity at the common boundary. At $\rho = \rho_c$ we must have

$$w_o = \bar{w}_o, \qquad w_n = \bar{w}_n \tag{35}$$

$$\partial w_o/\partial r = \partial \bar{w}_o/\partial r, \qquad \partial w_n/\partial r = \partial \bar{w}_n/\partial r \tag{36}$$

$$\partial^2 w_o/\partial r^2 = \partial^2 \bar{w}_o/\partial r^2, \qquad \partial^2 w_n/\partial r^2 = \partial^2 \bar{w}_n/\partial r^2 \tag{37}$$

$$V_o - \bar{V}_o = mP/2\pi\rho_c a, \qquad V_n - \bar{V}_n = mP/\pi\rho_c a \tag{38}$$

Substituting the appropriate expressions from Eq. (18) through (34) into Eqs. (35) through (38) and solving the resulting equations for the integration constants of the outer region in terms of those of the inner region, we have

$$\bar{A}_o = A_o + \frac{mPa^2}{8\pi D}\rho_c^2(1 - \ln\rho_c) \qquad \bar{A}_n = A_n - \frac{\rho_c^{-(n-2)}}{n(n-1)}\frac{mPa^2}{8\pi D} \tag{39}$$

$$\bar{B}_o = B_o - \frac{mPa^2}{8\pi D}(1 + \ln\rho_c) \qquad \bar{B}_n = B_n + \frac{\rho_c^{-n}}{n(n+1)}\frac{mPa^2}{8\pi D} \tag{40}$$

$$\bar{C}_o = C_o + \frac{mPa^2}{8\pi D}\rho_c^2 \qquad \bar{C}_n = C_n - \frac{\rho_c^{n+2}}{n(n+1)}\frac{mPa^2}{8\pi D} \tag{41}$$

$$\bar{D}_o = D_o + \frac{mPa^2}{8\pi D} \qquad \bar{D}_n = D_n + \frac{\rho_c^{n}}{n(n-1)}\frac{mPa^2}{8\pi D} \tag{42}$$

where

$$P = -\frac{p_o\pi(a^2-b^2)}{m} = -\frac{p_o\pi a^2(1-\rho_b^2)}{m} \tag{43}$$

The remaining eight equations for solving the integration constants are obtained from the boundary conditions.

Boundary Conditions

At the inner boundary, if $\rho_b = 0$ (no central hole), the plate deflection must be finite. Therefore, in view of Eqs. (18) and (26), we must have

$$C_o = D_o = C_n = D_n = 0 \tag{44}$$

If $\rho_b \neq 0$, the inner boundary is free. The outer boundary is also free. Therefore

$$M_{r_o} = V_{r_o} = M_{r_n} = V_{r_n} = 0 \text{ at } \rho = \rho_b \text{ and at } \rho = 1 \tag{45}$$

Substituting the appropriate expression from Eq. (18) through (34) into the boundary conditions (45) and using relations (39) through (42) between the integration constants of the two regions, we can obtain the required equations for solving the constants of the inner region.

n = 0: If $\rho_b = 0$, C_o and D_o are given by (44).

$$B_o = -\frac{p_o a^4}{32D}\left[\frac{(1+3\nu) + 2(1-\nu)\rho_c^2}{1+\nu} + 4 \ln \rho_c\right] \tag{46}$$

If $\rho_b \neq 0$,

$$B_o = -\frac{p_o a^4}{32D}\left[\frac{(1+3\nu) + 2(1-\nu)\rho_c^2 - (3+\nu)\rho_b^2}{1+\nu} + 4\left(\ln \rho_c + \frac{\rho_b^4}{1-\rho_b^2} \ln \rho_b\right)\right] \tag{47}$$

$$C_o = -\frac{p_o a^4 \rho_b^2}{16D(1-\nu)}\left[(1+3\nu) + 2(1-\nu)\rho_c^2 + 4(1+\nu)\left(\ln \rho_c + \frac{\rho_b^2 \ln \rho_b}{1-\rho_b^2}\right)\right] \tag{48}$$

$$D_o = -\frac{p_o a^4 \rho_b^2}{8D} \tag{49}$$

In both cases, since $w_o = 0$ at $\rho = \rho_c$, we have from Eq. (18),

$$A_o = -\left[B_o \rho_c^2 + C_o \ln \rho_c + D_o \rho_c^2 \ln \rho_c + p_o a^4 \rho_c^4 / 64D\right] \tag{50}$$

n = km ≥ 2: A_n and B_n can be obtained by solving the following two equations whether ρ_b equals zero or not.

$$A_n \frac{(n-1)(1-\nu)}{3+\nu}(1-\rho_b^{2n}) + B_n \frac{n^2(1-\nu)^2 + 8(1+\nu)}{n(1-\nu)(3+\nu)}(1-\rho_b^{2n+2})$$

$$= \frac{p_o a^4 (1-\rho_b^2)}{8nD}\left[\frac{n^2(1-\nu)^2 + 8(1+\nu)}{n(n+1)(1-\nu)(3+\nu)} \rho_c^{-n} - \frac{\rho_c^{n+2}}{n+1} - \frac{1-\nu}{3+\nu} \rho_c^{-(n-2)}\right] \tag{51}$$

$$A_n\, n(1-\rho_b^{2n-2}) + B_n (n+1)(1-\rho_b^{2n})$$

$$= \frac{p_o a^4 (1-\rho_b^2)}{8nD}\left[\rho_c^{-n} - \frac{n}{n-1} \rho_c^{-(n-2)} - \frac{3+\nu}{(n-1)(1-\nu)} \rho_c^n\right] \tag{52}$$

Then C_n and D_n can be obtained from

$$C_n = \frac{(1-\nu)(1-n)}{3+\nu} \rho_b^{2n} A_n - \frac{n^2(1-\nu)^2 + 8(1+\nu)}{n(1-\nu)(3+\nu)} \rho_b^{2(n+1)} B_n \tag{53}$$

$$D_n = \frac{1-\nu}{3+\nu} \left[n\rho_b^{2(n-1)} A_n + (n+1)\rho_b^{2n} B_n \right] \tag{54}$$

Support point deflection. After calculating the integration constants, the following deflection must be subtracted from $w(r,\theta)$ and $\bar{w}(r,\theta)$, so that the deflection at the support points become zero.

$$w_{sup} = \left[A_n \rho_c^n + B_n \rho_c^{n+2} + C_n \rho_c^{-n} + D_n \rho_c^{-(n-2)} \right] \tag{55}$$

Numerical Verification

The formal solution of the boundary value problem under consideration is now complete. For the multi-point mount problem, the integration constants in the inner region can be calculated from Eqs. (44) and (46) through (54), followed by the calculation of the integration constants for the outer region using Eqs. (39) through (43). The deflections and the stress resultants are then calculated from Eqs. (18) through (34). For convenience a computer routine was developed incorporating these equations, and a number of test cases were run for numerical correlation with independent computations from a NASTRAN based finite element model. The tests cases included circular flat plates with and without a central hole and with 3-point and 6-point supports at the outer boundary and at 70% of the outer radius. The correlation was excellent in all the cases. Figures 4 and 5 illustrates the results for two of these cases.

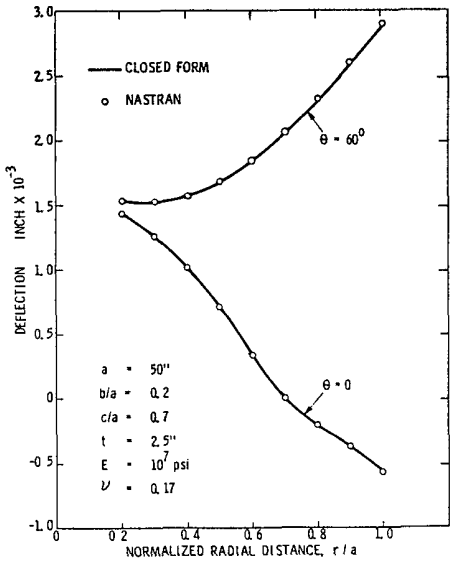

Figure 4. Comparison between closed form and Nastran solutions for a circular flat plate with a central hole on a 3-point support at 70% radius

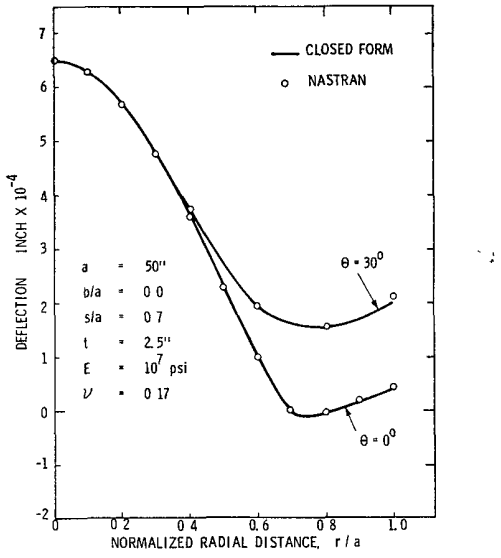

Figure 5. Comparison between closed form and Nastran solutions for a circular flat plate without a central holt on a 6-point support at 70% radius

As discussed earlier in the section on analytical approach, the theoretical solution for the 9-point Hindle mount problem is obtained from that of the multi-point mount problem by superimposing the solutions of three cases. In each case, the plate is supported on three points and subjected to a uniform pressure equal to $\mu_i W/\pi a^2(1-\rho_b^2)$ where μ_i (i = 1, 2, 3) is given Eqs. (4) through (6). The superposition algorithm was also implemented in our computer software for convenience and validated by running several test cases for numerical correlation with Nastran based finite element analysis.

The test cases included circular flat plates, with and without a central hole, supported on a 9-point Hindle mount with symmetric and nonsymmetric delta-plates. Figures 6 and 7 illustrate the results for two of these cases. The correlation between the two methods was excellent in all the cases.

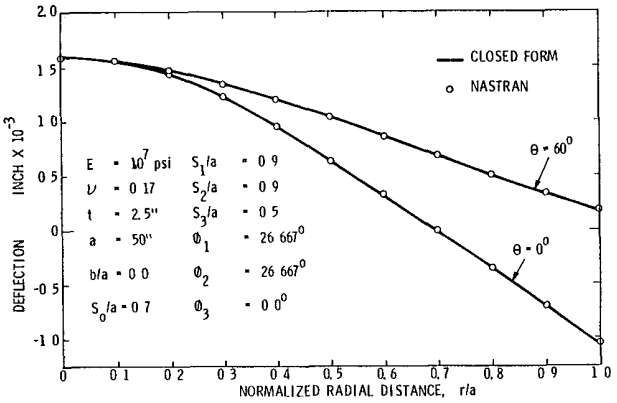

Figure 6. Comparison between closed form and Nastran solutions for a circular flat plate without a central hole on a 9-point Hindle mount with symmetric delta-plates

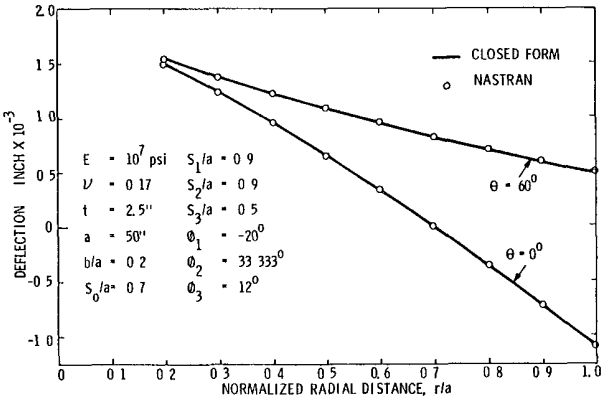

Figure 7. Comparison between closed form and Nastran solutions for a circular flat plate with a central hole on a 9-point Hindle mount with nonsymmetric delta-plates

A design approach

We will now apply the 9-point Hindle mount solution and the associated computer software to develop normalized design curves for the support locations and RMS figure error. It was assumed earlier that each of the three delta-plates supports one-third of the weight of the circular plate, or W/3. For the proposed design approach, it is further assumed that each of the three floating supports, located at the vertices of a delta-plate, nominally takes one-third of the load on the delta-plate, or W/9. Recalling that in the nominal case (symmetric delta-plates), $s_1 = s_2$ and $\phi_1 = -\phi_2$ (see Figures 1 and 2), the last assumption leads to the following kinematic constraint among the radial and angular locations of support points by virtue of moment equilibrium of the delta-plate.

$$s_o - s_3 = 2(s_2 \cos \phi_2 - s_o), \quad \text{or} \quad s_2 \cos \phi_2 = (3s_o - s_3)/2 \tag{56}$$

Since there are four unknowns, s_o, s_2, s_3 and ϕ_2, three more equations are required besides Eq. (56) for determining the support locations. Ideally, these equations may be obtained by deriving an expression for RMS figure error as a function of the four unknowns, eliminating from it one of the four unknowns by means of Eq. (56), and equating the partial derivatives of the function with respect to each of the remaining three unknowns to zero. The resulting equations would be nonlinear, transcendental and, generally speaking, untractable. Fortunately, since the computer software developed above for the convenience of rapid calculations is extremely economic to run and takes only a very small fraction of computing time per run taken by the finite element analysis, an alternative approach based on a computer search for the minimum RMS figure error is possible. The search was carried out in two steps.

First, the radius s_o of the three fixed supports (i.e. delta-plate centroids) was determined by numerical variation of its value until the RMS deflection of the circular plate on a 3-point support became minimum. The normalized radius s_o/a of the delta-plate centroid so determined is plotted versus the normalized central hole radius b/a in Figure 8 for several values of the Poisson's ratio ν. Admittedly, this is not an optimum but rather a workable choice of s_o.

Next, for any given value of s_o determined above, s_2 and s_3 were numerically varied in small increments ($\pm i\Delta s_2$ and $\pm j\Delta s_3$, for i = 1, 2, 3,..., i_{max} and j = 1, 2, 3,....., j_{max}), while ϕ_2 was calculated from Eq. (56), until the RMS deflection of the circular plate on a 9-point Hindle mount became a minimum. The results of this computational search for the floating support locations are plotted versus the normalized central hole radius

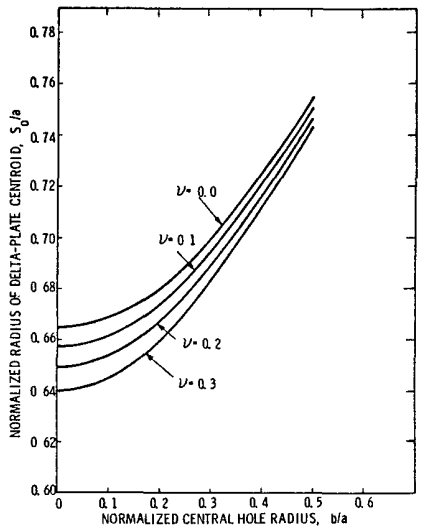

Figure 8. Variation of normalized radius of the delta-plate centroid with normalized central hole radius and Poisson's ratio ν

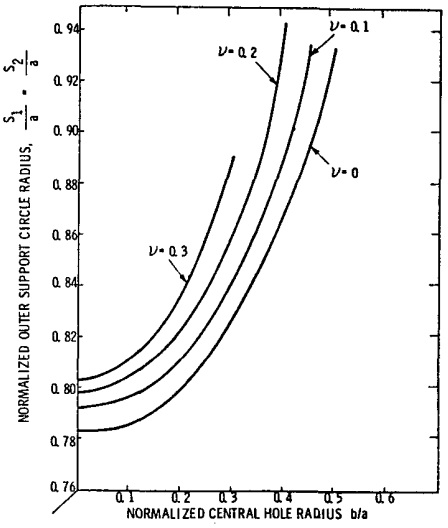

Figure 9. Variation of normalized outer support circle radius with normalized central hole radius and Poisson's ratio ν

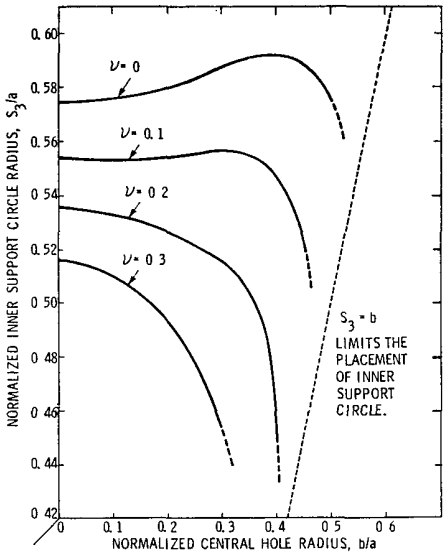

Figure 10. Variation of normalized inner support circle radius with normalized radius of the central hole and Poisson's ratio ν

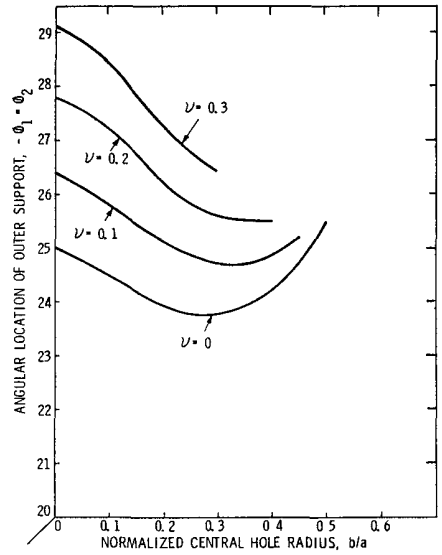

Figure 11. Variation of the angular location of outer supports with normalized central hole radius and Poisson's ratio ν

b/a in Figures 9 through 12 for several values of the Poisson's ratio. Figure 13 and 14 give similar plots of the normalized RMS deflection and the induced radius of curvature of the best fit sphere, respectively.

The normalized design curves of Figure 8 through 13 provide the design engineer with a useful means of rapidly configuring a preliminary 9-point Hindle mount design for flat circular optical elements made of materials with linear elastic properties. This approach may not be optimum for two reasons. The assumed load distribution between the inner and outer floating supports and the determination of the delta-plate centroid given in Figure 8 may not be optimum. However, the proposed approach, in combination with the support location sensitivity analysis of the next section, is quite useful, accurate and fast in practice. Further, the flat circular plate solution for the 9-point Hindle support given in this paper can be easily programmed and used to compute the RMS figure error for any other 9-point Hindle mount design outside the framework of these design charts.

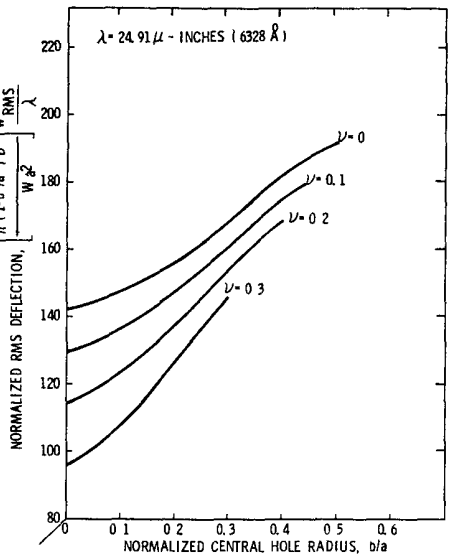

Figure 12. Variation of normalized RMS deflection with normalized central hole radius and Poisson's ratio ν

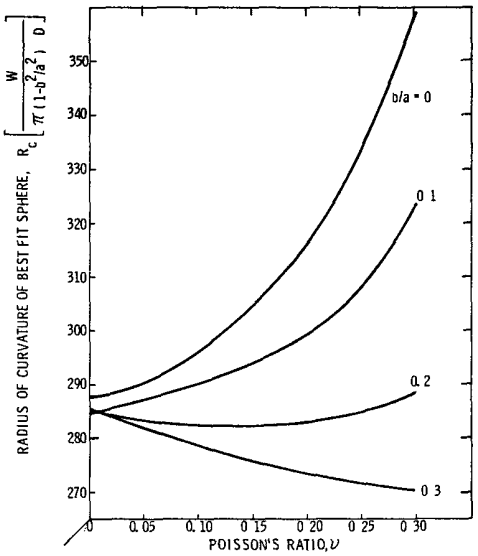

Figure 13. Variation of normalized radius of curvature of the best fit sphere with Poisson's ratio ν and normalized central hole radius

Sensitivity analysis

When the location of a floating support in any delta-plate is perturbed, the load distribution is changed. The support forces, instead of all being equal to W/9, are equal to $\mu_i W/3$, where μ_i are given by Eq. (4), (5) and (6). In the sensitivity analysis, the radial and angular position of each floating support was perturbed separately and the resulting effect on the figure error was computed. From this, location sensitivity charts were prepared. These charts are shown in Figures 14 through 17. For several values of

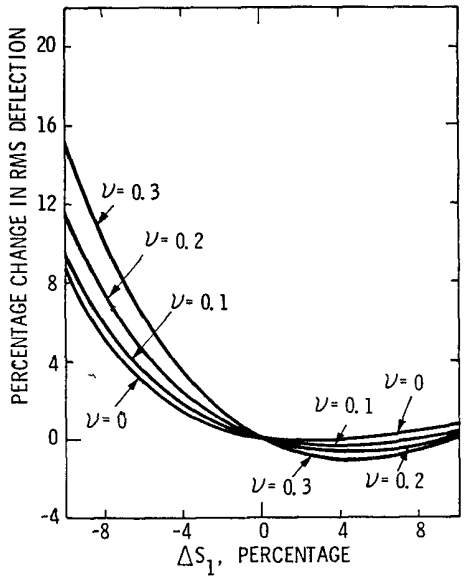

Figure 14. Sensitivity analysis chart for radial location s_1 of the outer floating supports

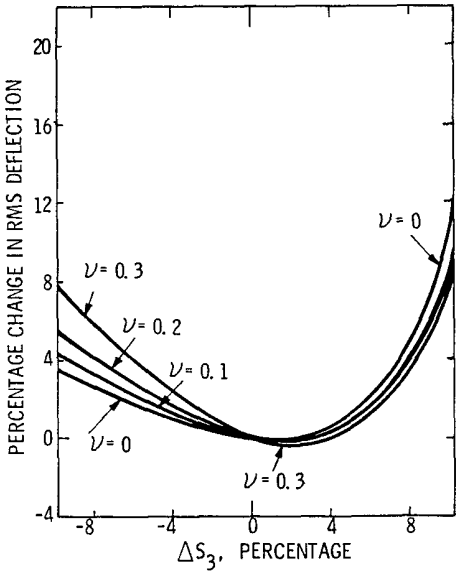

Figure 15. Sensitivity analysis chart for radial location s_3 of the inner floating supports

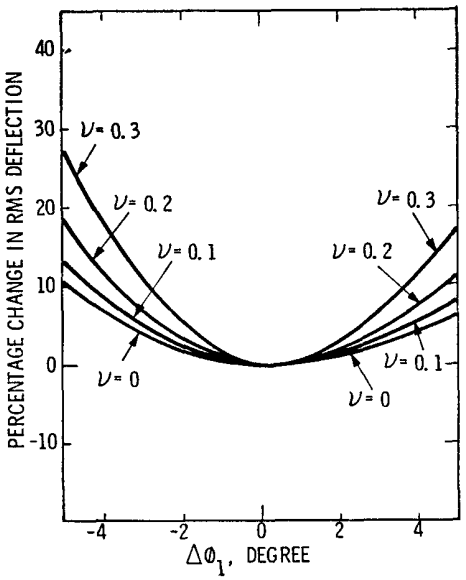

Figure 16. Sensitivity analysis chart for angular location ϕ_1 of the outer floating supports

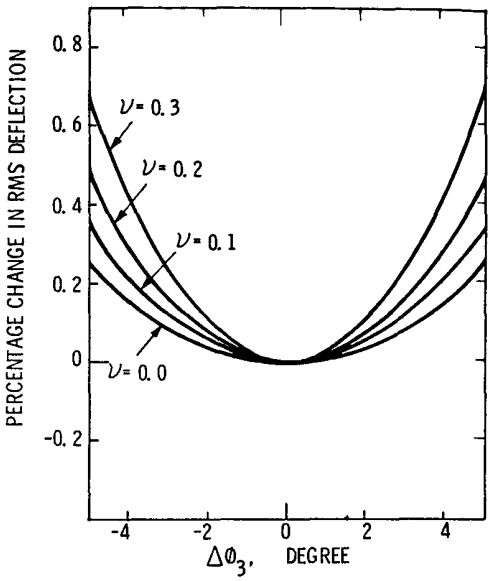

Figure 17. Sensitivity analysis chart for angular location ϕ_3 of the inner floating support

Poisson's ratio, the sensitivity charts give the percentage change in the nominal RMS deflection as a separate function of change in each of the radial and angular positions of the outer and inner floating supports, respectively. It can be seen from these charts that the RMS deflection is most sensitive, and also significantly so, to small angular location changes ($\pm$ 5°) in outer floating supports (see Figure 16). On the contrary, it is least, almost negligibly, sensitive to similar changes in the inner floating support (see Figure 17). The design engineer may use these charts to establish location tolerances and estimate the worst case RMS figure error in any suitable way. The RMS figure error for coherent combinations of location tolerances can be calculated by using the 9-point Hindle mount solution for nonsymmetric delta-plates. The sensitivity analysis for the fixed support (delta-plate centroid) location still remains to be done.

Concluding Remarks

For flat circular optical elements supported on 9-point Hindle mounts and subjected to uniform loading due to its own weight, the normalized design curves and sensitivity charts provide the design engineer with a useful, efficient and accurate means for configuring a preliminary mount design. For a 9-point Hindle mount outside the framework of the design charts, the closed form solution and the computer software, based on it, can be used. This software is extremely economic to run in comparison with a finite element model of the plate and is equally accurate.

The method used for the solution of the basic m-point support case is applicable to shallow spherical shells represented by E. Reissner's equations[2]. In fact this work is currently in progress and will be published in the future. The m-point solution can be applied to multi-level Hindle mounts with 18, 27, 36, and 81 supports, etc. The effect of transverse shear flexibislity may be included for light-weighted cross section either by adding on or by considering appropriately modified differential equations[3] for combined bending and shear and applying it to the Hindle mount problem in a similar fashion. The method of solution used in this paper is also applicable to other types of loads, such as a point force due to an adaptive optics actuator at an arbitrary location.

In these times of mushrooming FEM technology, there is a tendency to resort to finite element analysis as a panacea for everything. Quite often during the early stages of a project, when a trade-off study needs to be made as an aid to concept evolution and development of a preliminary configuration, or a quick response to a technical question is required, the finite element analysis may not be cost-effective and/or convenient. On the other hand, the cookbook types of formulas available in some handbooks most often represent too crude an approximateion of the problem on hand to be sufficiently reliable. Fortunately, there are a number of problems in opto-structural mechanics that can be cost-effectively tackled by the classical methods of engineering mechanics. It is hoped that this paper serves as a demonstration of this viewpoint to some extent.

Acknowledgments

The work presented in this paper was funded by an IR&D program of the Perkin-Elmer Corporation.

References

1. Marquerre, K. and Woernle, H., Elastic Plates, Blaisdell Publishing Company, 1969.
2. Kraus, H., Thin Elastic Shells, John Wiley & Sons, Inc., 1967.
3. Reissner, E., "The Effect of Transverse Shear Deformation on the Bending of Elastic Plates", J. Appl. Mech., pp A70-A77, June 1945.